Estimating Surgical Needle Deflection with Printed Strain Gauges

Frank L. Hammond III, *Member, IEEE,* Michael J. Smith, and Robert J. Wood, *Member, IEEE*

***Abstract*—The ability to track surgical needle deflection during procedures such as therapeutic drug delivery, biopsies, and medical device implantation allows clinicians to minimize positioning errors and procedural complications due to instrument deviations. We describe the use of a novel strain gauge printing method to sensorize surgical needles for the purpose of sensing needle shape and deflection during surgical procedures. The additive vapor-deposition based sensor fabrication method used here is capable of applying strain gauges (and resistive circuit elements) with micron-scale features onto surgical instruments of varying curvature and material composition without the need for mechanical machining. This fabrication method is used to apply several strain gauges onto an 18 gauge core biopsy needle to sense deflections. Validation experiments demonstrate a gauge factor of 1.16 for the printed strain gauges and nominal needle deflection measurement resolution of 500 microns.**

I. Introduction

The deflection of surgical instruments due to interaction forces (anywhere from 5mN to 50N) is an expected but nonetheless problematic during clinical procedures. Instruments such as forceps, needle drivers, and biopsy needles [1-4], and devices such as hemostats, retractors, and catheter tips can experience relatively large strains during use. These strains can lead to errors in instrument positioning which can decrease the efficiency and quality of surgical tasks which can, in turn, lead to procedural complications and decreased quality of treatment [5]. The ability to detect and compensate for such instrument deflections is critical to the improvement of invasive clinical procedures, both diagnostic and therapeutic.

Attempts have been made to install force sensors on various surgical instruments for the purpose of sensing deflection and enabling haptic feedback. Force sensing technologies include embedded optical fiber-Bragg grating (FBG) sensors [6], soft liquid-embedded tactile sensors [7], and silicon based strain gauges [8,9]. These solutions, though effective in research experiments, have proven prohibitively expensive and technically difficult to implement in practice due to costly sensor fabrication processes (FBG sensors), sensor installation challenges (mounting compliant sensors to rigid tools using adhesives or machining grooves or mating features into instruments to mount fiber optics), and manufacturing complexity (wiring, signal conditioning, and data acquisition hardware).

Manuscript received April 7, 2014, final paper submitted on June 16, 2014. F. L. Hammond III, M. J. Smith, and R. J. Wood are with the Harvard School of Engineering and Applied Sciences, 60 Oxford Street, Cambridge, MA 02138 USA (email: fhammond@seas.harvard.edu).

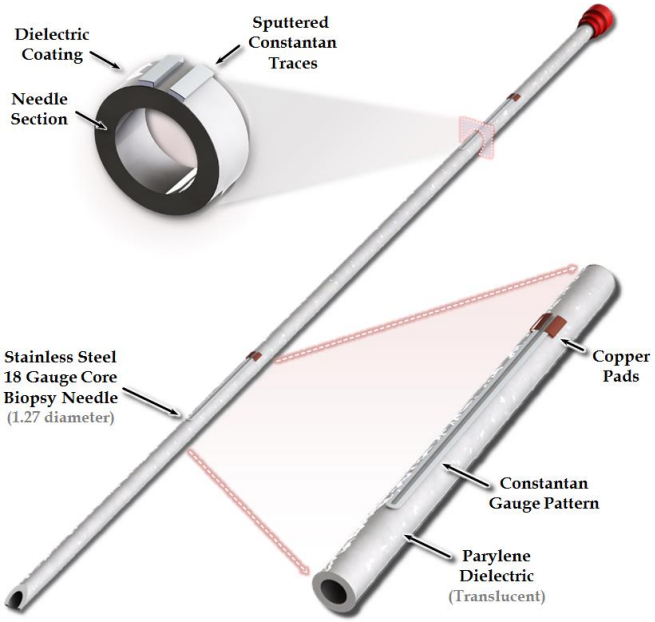

Fig. 1. A model of a strain gauge designed to be printed onto an 18 gauge cope biopsy needle to sense needle deflections. A section of the needle and strain gauge (top-left) and close-up of the gauge (lower right) are shown.

In contrast to conventional strain gauge technologies, the technology we present here is a topical, deposition-based process which eliminates the need for instrument machining, complicated surface treatments and adhesives, and the need for wiring and attachment of signal conditioning circuit components necessary for strain measurement. This non-contact manufacturing process leverages chemical vapor deposition (CVD), physical vapor deposition (PVD) and precise laser machining technologies to print highly-sensitive metallic strain gauges directly onto instrument surfaces of varying material composition and curvature. This process has the advantages of (1) inexpensive fabrication, (2) flexibility of sensor design (out-of-plane), and (3) ability to print gauges onto pre-existing instruments, eliminating the need to design specialized instruments to sense forces.

In this paper, the proposed technology is used to print a strain gauge onto a 18 gauge core biopsy needle (Fig. 1) for the purpose of estimating needle deflection under expected interaction forces. This work demonstrates both the versatility of the strain gauge printing process by sensorizing a commercially available device of small size and high-curvature (1.27mm outer diameter needle) and the sensitivity of the resulting strain gauges by accurately measuring hundreds of microns of needle lateral deflection. Section II describes the design and analysis of the strain gauge used to measure needle deflection. Section III describes the strain

gauge printing process and the fabrication of a prototype gauge on a needle. Section IV details the testing of the sensorized needle under expected interaction forces. Section V summarizes the experimental results, and Section VI discusses conclusions and future research directions.

II. Strain Gauge Design

A. Needle Deformation Mechanics

The 18-gauge core biopsy needle sensorized using the proposed printed strain gauge process will most likely experience cantilever bending modes in clinical practice, where that base of the needle is fixed to a needle driver (robotic and manual) and interaction forces are imparted at the needle tip during tissue penetration and steering. For the purpose of design and experimental validation, we will assume that these interaction forces are comprised of a point load concentrated at the distal tip and that the force is normal to the central axis of the needle (Fig. 2). We also assume that deflection at the needle base is zero, that curvature at the needle tip is zero, and that total tip deflection is less than 10% of the total needle length (15cm in this case) such that small-strain linear beam theory applies [10].

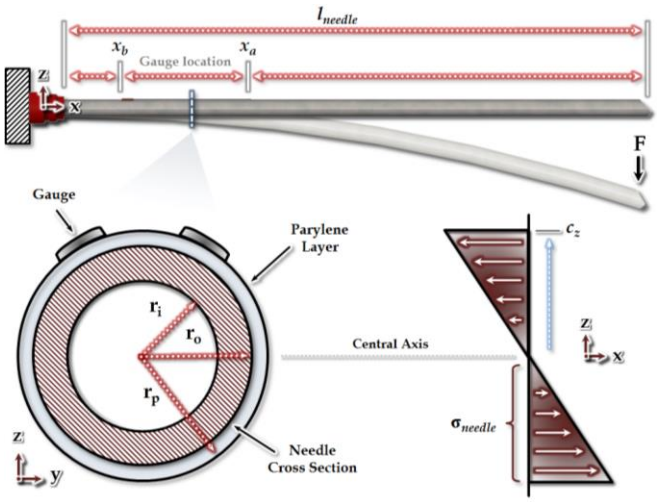

Fig. 2. The mechanical model and stress-strain behavior of the core biopsy needle, with Parylene coating and strain gauge printed onto the surface, under cantilever loading conditions.

The cross-sectional dimensions of the biopsy needle are an inner radius r_i of 0.42mm and an outer radius r_o of 0.635mm, assumed constant throughout the needle length l_{needle} of 150mm, resulting in a second area moment I_{needle} of 6.4537 x 10^{-15} m^4 (1). The needle is comprised of austenitic 316 stainless steel with an elastic modulus E_{ss} of 205 GPa and a Poisson's ratio $\nu = 0.275$. The printed strain gauge and all constituent components are assumed to deform with the needle given that the second area moment of the strain gauge is much less than that of the needle.

$$I_y = \frac{\pi}{4}\left(r_o^4 - r_i^4\right) \tag{1}$$

B. Strain Gauge Design Analysis

The topology of the printed strain gauge used for needle deflection measurement is shown in Fig. 3 as a 10mm long U-shaped trace made of constantan – an alloy consisting of 55% copper and 45% nickel - aligned along the axis of the needle. The strain gauge design has several variables, including trace width w_{tr}, trace thickness t_{tr}, trace separation (and radius of trace turn) d_{sep}, the location of the gauge given by endpoints x_a and x_b, and trace length given by the distance $x_b - x_a$. Here, we set trace length at 10mm, w_{tr} at 150µm, d_{sep} at 150µm, and trace thickness at 900nm and vary only the position of the strain gauge along the needle shaft.

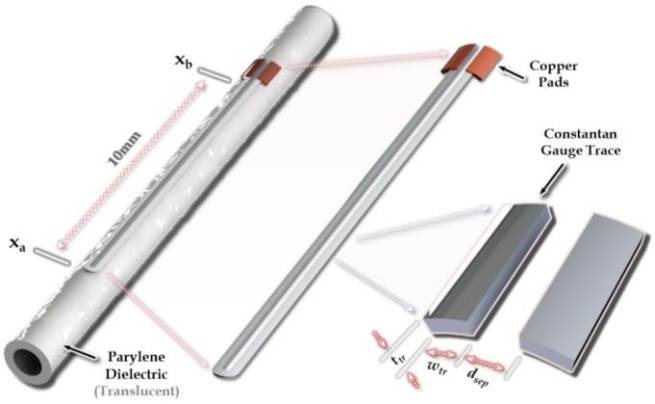

Fig. 3. The topology and dimensions of the proposed printed strain gauge shown with a section view of the 18 gauge core biopsy needle. Though curved on the needle surface, the gauge is assumed flat for predictions.

The strain gauge must have a gage factor high enough to respond to needle deflections under expected loading conditions and must also have a topology and location on the needle such that the resulting strain does not exceed the gauge material's mechanical limits. We assume here that strain throughout the thickness of the strain gauge is equivalent to that at the outer needle surface, given the low profile of the printed gauges relative to their radial distance from the line of action, their volume relative to that of the needle, and the strong interface bond between the gauge Parylene, and the needle. Proper gauge placement ensures safe, non-destructive strain gauge deformations while providing adequate sensitivity to needle deflection.

Placement of the gauge requires estimation of the strains induced by bending of the needle under cantilever loading. The bending strain at a point x_i on the surface of the needle is given by (2), where the moment M_i is the product of the interaction force F at the needle tip and the distance of point x_i from the needle tip (Fig. 2). The total change in surface length is given by integral in (3) where the distance between points x_a and x_b is the length of the strain gauge.

$$\varepsilon = \frac{M_i z}{EI} = \frac{F x_i z}{E\left(\frac{\pi}{4}\left(r_o^4 - r_i^4\right)\right)} \tag{2}$$

$$\Delta l = \int_{x_a}^{x_b} \frac{Fxz}{EI} dx \; ; \; x_a = \left(l_{needle} - x_f\right), \; x_b = \left(l_{needle} - x_a\right) \tag{3}$$

The corresponding change in gauge resistance is given by (4) and the theoretical gage factor is given by (5), where R is nominal strain gauge resistance, ρ is constantan resistivity, and A is the cross-sectional area of the gauge.

$$\Delta R_{gauge} = \frac{\rho}{A}\int_{x_o}^{x_f}\left\{\frac{\left(1+\frac{Flz}{IE}\right)}{\left(1-\nu\frac{Flz}{IE}\right)^2}-1\right\}dl \qquad (4)$$

$$S_{gauge} = \frac{\Delta R/R}{\varepsilon} = \frac{\Delta R\cdot(x_f - x_i)}{R}\left\{\int_{x_a}^{x_b}\frac{Flx}{EI}dx\right\}^{-1} \qquad (5)$$

Using the above equations, we determine the strain gauge locations that limit maximum strain while maximizing gage factor. Figure 4 plots the theoretical maximum gauge strain σ_{max} and gage factor (GF) versus placement for a cantilever load of 1N - well under the 3.543N which causes the maximum deflection (15mm) allowable under small-strain linear beam theory. Results show a suitable gauge position is greater than 4.5cm from the needle base (<9.5cm from tip).

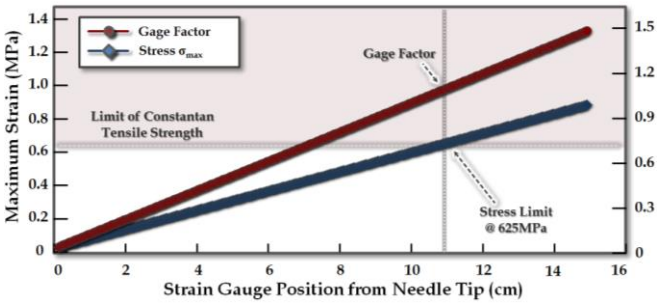

Fig. 4. Theoretical maximum strain and gage factor of the proposed printed strain gauge design at various positions along the needle length. Left y-axis shows maximum strain, right y-axis shows resulting gage factor. The x-axis position is the location of point x_a from the needle tip (Fig. 2).

III. Strain Gauge Sputtering Process

The strain gauge printing process involves several steps including (1) conditioning of the instrument surface, (2) dielectric insulation (3) selective surface masking, (4) deposition of multiple structural and functional material layers comprising the circuit components, and (5) a final protective coating (Fig. 5). First, the metallic surface of the needle is cleaned in a 1% solution of A-174 Silane in isopropyl alcohol and deionized water for five +hours (Specialty Coating Systems Inc., Indianapolis, IN, USA). This etches away any contaminants (e.g. residues from handling, oxidation layers) on the surface. The surface is then coated with several microns-thick layers of Parylene C, a moisture resistant, low permittivity polymer. This coating acts as a substrate layer for other material deposited during the printing process electrically insulating the metallic surface of the needle from the strain gauge. Parylene coating is done using a PDS 2010 Parylene deposition system (Specialty Coating Systems Inc.) which can create even coatings on surfaces of varying curvature and size.

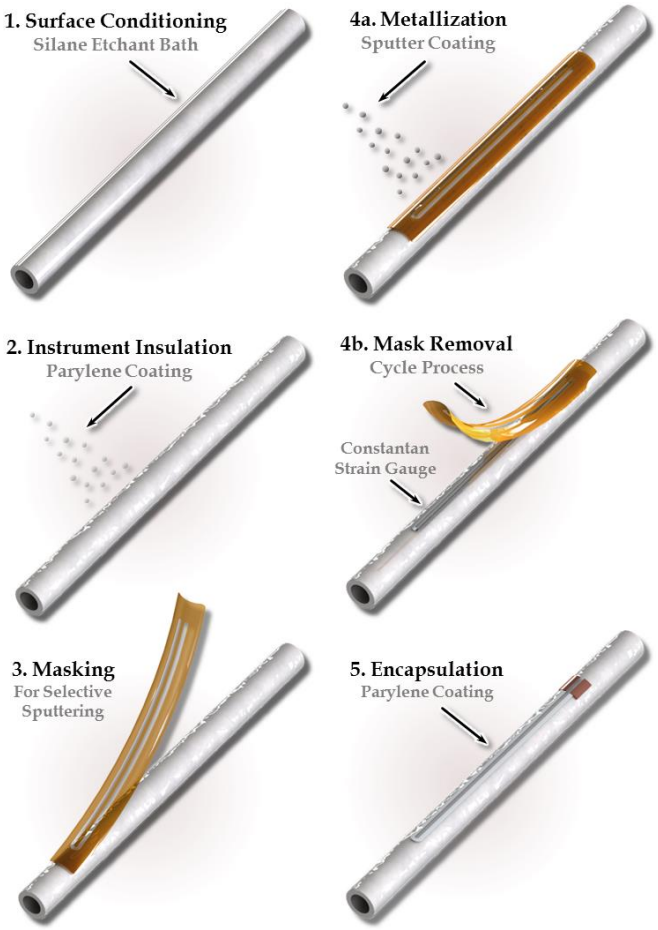

Fig. 5. Illustration of the five-step, vapor-deposition based printed strain gauge fabrication process.

After Parylene coating, sputtering masks with micron-sized features of the strain gauges are laser-cut from Kapton polymide tape (DuPont Co., Wilmington, DE, USA) and tacked onto the surfaces where the strain gauge layers will be deposited. With the sputtering masks in place, the constantan metal used for the strain gauge and the copper used for electrical traces are deposited onto the surfaces using a physical vapor deposition chamber (Denton Vacuum LLC, Moorestown, NJ, USA) at a rate of approximately 51.1 nm/min. Kapton masks are replaced and superimposed over several sputtering cycles to create the constantan strain gauge and copper pads for wiring. After deposition of the strain gauge and its pads, the needle surface is coated again in Parylene to insulate the gauge for biocompatibility and safety in clinical environments (including sterilization).

The strain gauge prototype is shown in Fig. 6 printed in the surface of 18 gauge stainless steel metal tubing (same dimensions and material as core biopsy needles), which serves as a surrogate for biopsy needle. The inset image shows the constantan trace and copper pads which were deposited in separate sputter runs. The final coating of Parylene, which is normally applied as a protective coating, was not applied to the prototype in order to allow for ease of wiring and imaging for validation. The nominal resistance of the strain gauge was 15.85kΩ (75.82Ω predicted).

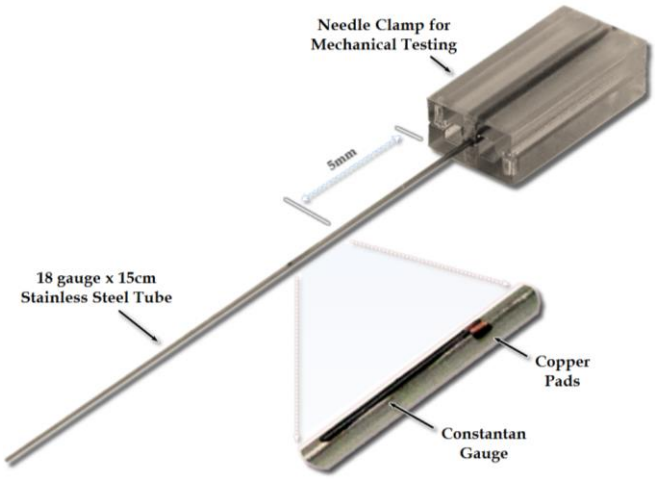

Fig. 6. Photo of completed strain gauge printed on 18 gauge stainless steel tubing, 5.0cm from the base (greater than the 4.5cm minimum), and mounted in a rapid prototyped clamp for electromechanical testing.

IV. Experiments

A. Electromechanical Testing

Experimental validation of the printed strain gauge was conducted using an Instron 5540 Series electromechanical testing system (Instron Inc., Norwood, MA USA). The sensorized biopsy needle was mounted in a cantilever configuration using a rapid prototyped needle clamp (Fig. 5). The strain gauge was connected to test equipment by 28 gauge copper wire, which itself was attached to the gauge's copper pads using silver epoxy. The Wheatstone bridge circuit (Fig.7) is balanced with 22kΩ resistors to measure the resistance changes in the gauge. The gauge leg of the bridge has a nominal resistance of 24.58kΩ, likely increased by parasitic resistance in the silver epoxy and wiring.

The needle was loaded with forces up to 0.15N at a rate of 10mm/min controlled tip deflection. The resistance changes in the strain gauge were measured with the Wheatstone bridge circuit and amplified using an LM2904N operational amplifier a non-inverting differential configuration (Fig. 7). Resistors R_a and R_b are set to 10kΩ and 1MΩ for a gain of 101. Measurements were acquired using a National Instruments DAQ at 10 Hz.

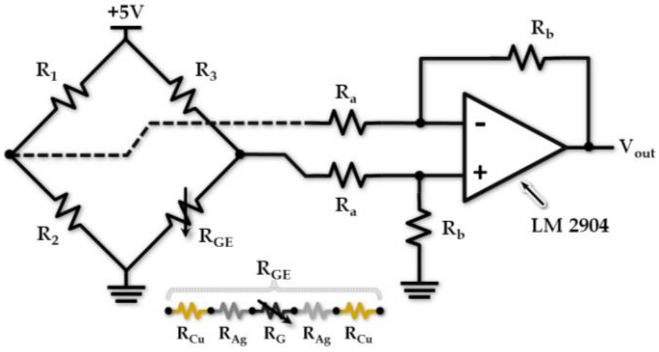

Fig. 7. Amplification circuit used for data acquisition, where R_{Cu}, R_{Ag}, and R_G is resistances of the copper wire, silver epoxy, and constantan strain gauge respectively. R_{GE} is the total resistance on the gauge leg of the bridge.

B. Off-Axis Deflection Sensitivity

The needle was first clamped and loaded with the strain gauge facing up, perpendicular to the Instron load frame and parallel to the ground (0° configuration). This configuration puts the strain gauge in tension and induces maximum strain during needle deflection (Fig. 8). In practice, alignment of the bending axis with the gauge will likely result in lower-than-maximum strains and would not provide knowledge of directionality of deflection. Additional strain gauges could be placed around the circumference of the needle to estimate both the magnitude and direction of deflection [6].

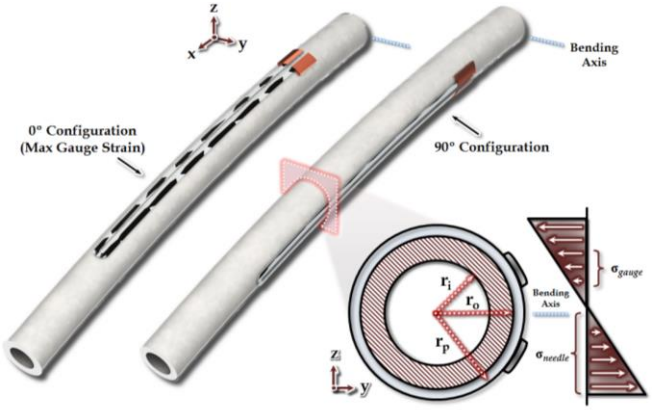

Fig. 8. Illustration of the two needle configurations experimentally tested for maximum strain and off-axis strain sensitivity. The lower right of the figure shows the distribution for the 90° gauge configuration.

As a preliminary test of the off-axis sensitivity of the strain gauge to needle deflections at different angles (askew of the x-axis or most sensitive bending direction of the strain gauge), the needle is also rotated by 90° and loaded similarly. In theory, the 90° configuration should exhibit much smaller responses to needle tip deflection than the 0° configuration given the decreased distance of the gauge trace from the bending axis. The sensitivity to bending axis orientation should allow the estimation of bending direction.

V. Results

The data in Figure 9 shows that the printed strain gauge output is linear and matches predicted performance in magnitude for small deflections. The experimental gage factor is 1.16. The slope of the output, however, is smaller at 5mV/mm deflection than the predicted output of ~10mV/mm deflection. The disparity may be attributed to several fabrication process variants and modeling assumptions discussed in the next section.

Figure 10 shows the strain gauge output with respect to tip deflection and needle orientation. The results clearly show that the orientation of the gauge, with respect to the bending axis, affects the gauge sensitivity. Based on this result, multiple strain gauges could be oriented about the circumference of the needle accurately to sense both the magnitude and direction of needle tip deflection given a proper calibration matrix calculation for the sensor group.

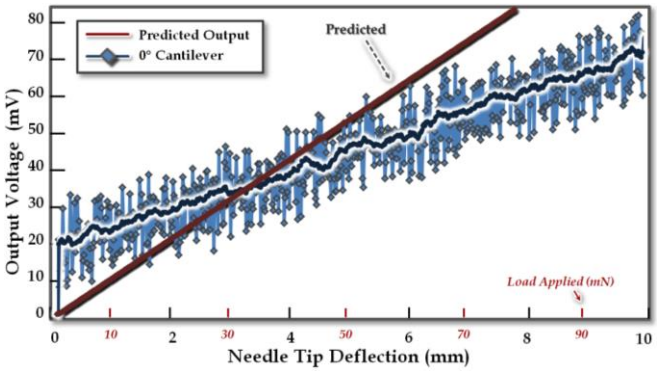

Fig. 9. Amplified strain gauge output of the needle with a 0° configuration and versus predicted strain gauge output for a gauge with a 75.82Ω nominal resistance in a perfectly balanced Wheatstone bridge.

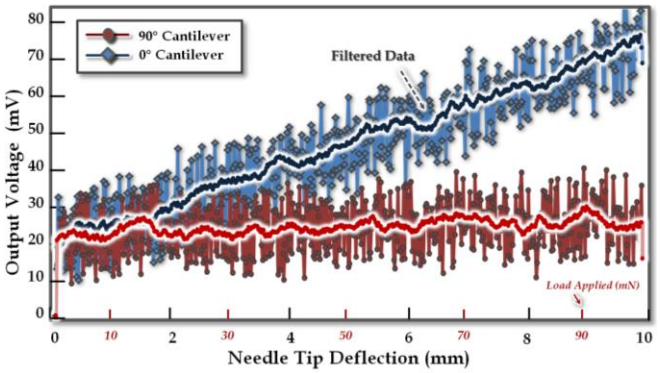

Fig. 10. Plot of amplified strain gauge output of the needle with a 0° configuration (gauge facing up and parallel to bending axis – maximum theoretical strain) and with a 90° configuration (gauge normal to bending axis – minimal strain). Applied load is shown on X-axis.

The voltage response of the strain gauge is repeatable and does not decay significantly over several loading cycle. This indicates that the printed strain gauge does not experience stresses beyond the tensile limit, which would fracture the gauge trace and cause permanent resistance increases. The exact amount of strain in the gauge during needle deflection, however, is difficult to discern given the parasitic resistance of the instrumentation and wiring, and process variations (sputter occlusion and oxidation).

VI. Discussion

A. Effect of Test Conditions on Performance

The needle deflection tests show that the printed strain gauge response was very similar in trend to the predicted response but differed in the expected resistance change. The expected voltage output of the amplification circuit due to needle deflection (and surface strain) was much lower magnitude than expected. Some of this disparity can be attributed to the fabrication process, where the sputtering of the metals through the Kapton masks creates rounded trace edges, rather than straight edges as predicted, due to line-of-sight occlusions from the mask height and the curvature of the needle. The nominal resistance is higher than predicted as the cross sectional area of the trace is not as large due to the decreased material deposition. Some of the discrepancy can also be attributed to the gauge deformation model, which assumes a flat gauge rather than a slightly curved one.

Another contributing factor to the gauge output magnitude is the quality of the electrical connections. The wires used for testing were connected to the strain gauges by silver epoxy, which after curing holds the wires in contact with the gauge contact pads. If the wires lose contact with the pads during epoxy deposition or curing, the current would flow only though the epoxy, which has much higher resistance (ρ_{AG} = 0.017 Ω·cm) than copper. This loss of wire-pad contact apparently occurred during test setup as the nominal gauge resistance was 15.85kΩ before the connection and 24.58kΩ after connection. This increased resistance served to decrease the sensitivity of the amplification circuit to strain gauge resistance changes, given that the bridge circuit was balanced against the total resistance of the gauge and wiring.

Yet another possible contributor to the unexpectedly high nominal resistance and smaller than expected strain gauge output is material properties intrinsic to sputtered metals. The microstructure of vapor-deposited thin films and the corresponding electrical properties are known to be affected by the sputtering power, distance, and pressure [11]. The effects of these on the process variants are unknown and must be studied further to improve process reliability and fabrication controllability.

B. Printed Strain Gauge Performance Comparison

Despite sensitivity issues due to noise and bias in the test instrumentation, the printed strain gauge provided enough sensitivity to measure hundreds of microns of needle deflection. Figure 9 shows the strain gauge output over the total needle tip deflection range. A 500 micron deflection induced a 6.4 mV response, through the amplification circuit in Fig. 7. The signal to noise ratio (SNR) of the raw strain gauge circuit output, taking the noise amplitude against a linear fit to the output data, was 6.739. The SNR for filtered strain gauge output data was 88.61. The minimum detectable signal (MDS) threshold for this strain gauge was computed as the root mean square error (RMSE) of the output, which is 1.45mV. This voltage output was converted to a minimum detectable strain by taking the MDS over the linear data fit slope m_{fit}, which yields a minimum measurable tip deflection δ_{min} of 267.4 microns. Using tip deflection δ_{min}, the strain gauge position from the needle tip x_a, and the MDS, the total gauge strain at minimum detectable deflection is computed using (4) as 15.093 x 10^{-5}, or 15.093με (microstrain).

$$MDS = RMSE(y_{data} - y_{fit})\ ;\ \delta_{\min} = RMSE \cdot m_{fit}^{-1} \qquad (6)$$

A comparison of the printed strain gauge performance to the best-case performance of commercial strain gauges [12] is shown in Table I. The gauge factors of the printed strain gauge and commercial foil gauges are of similar order, but the MDS of the printed gauge is an order of magnitude lower. This disparity can be attributed to instrumentation noise and biases described in Section VI-A.

TABLE I
PRINTED STRAIN GAUGE CIRCUIT PROPERTIES

Property	*Printed Gauge* *Experimental*	*Foil Gauges* *Commercial*	*Silicon Gauges* *Commercial*
Gage Factor	1.16	2.0-4.0	75-175
SNR	88.04	NA	NA
MDS (με)	15.09	300	1500

The gage factor is computed from experimental data. SNR is the signal to noise ratio and MDS is the minimum detectable signal, represented here by induced microstrain. SNR and MDS are influenced by measurement conditions and are not indicative of best case performance as are the numbers for foil and silicon strain gauges, which are taken from [12].

An amplification circuit with a higher gain and improved output signal filtering could produce the hundreds of mVs responses and provide the noise rejection necessary for decreasing the minimum detectable strain of the printed strain gauge and enabling more accurate deflection measurement comparable to that seen in commercial foil gauges. The printed strain gauge sensitivity cannot be increased to the level of silicon strain gauges due to intrinsic material property limitations, but it has the advantage of higher maximum strain rates – up to 5% for foil and printed vs <1% for silicon, depending on thickness [13].

VII. CONCLUSION

This paper introduces a novel, vapor-deposition based fabrication process capable of printing strain gauges on medical instruments of varying geometry and composition for the purpose of force sensing and deflection measurement. We printed a small strain gauge (450µm x 10mm) with micron-sized features onto a common surgical instrument – a core biopsy needle - and obtained a gage factor of 1.16, allowing us to register 100's of microns of tip deflection. Though this gage factor is much less than those seen in commercial foil gauges (2.0-2.2), the ability to customize the strain design in the process by laser-machining new Kapton masks makes it possible to increase the gage factor (e.g. by increasing gauge length) in future designs.

The experimental validation of the strain gauge printed on the 18 gauge biopsy needle highlighted both the capability of this novel gauge printed process to apply highly sensitive gauges to small, high curvature instruments without need for machining or adhesives, and the vulnerability of this process to wiring and instrumentation challenges – a drawback for all conventional strain gauge technologies.

Future work on printed strain gauges will focus on refining the fabrication process for faster and more repeatable printing (more even deposition of strain gauge materials), as well as the expansion of the printing capabilities to include more sophisticated circuit components. Many of the instrumentation challenges faced in this work can be mitigated by printing signal conditioning circuitry, wireless communication, and inductive powering components directly onto instruments along with the strain gauges to eliminate the need for contact-based wiring and instrumentation. Efforts are being made to increase process versatility and enable these new printing capabilities.

ACKNOWLEDGMENT

The authors gratefully acknowledge the Wyss Institute for Biologically Inspired Engineering for its support of this research. Any opinions, findings, and conclusions or recommendations expressed in this material are those of the authors and do not necessarily reflect the views of the Wyss Institute. F. L. Hammond III thanks the National Academy of Sciences for financial support through the Ford Foundation Postdoctoral Fellowship Award.

REFERENCES

[1] A. Okamura, C. Simone, and M. O'Leary, "Force modeling for needle insertion into soft tissue," *IEEE Transactions on Biomedical Engineering*, vol. 51, no. 10, pp. 1707-1716, 2004.

[2] R. Webster, J. Memisevic, and A. Okamura, "Design considerations for robotic needle steering," *IEEE International Conference on Robotics and Automation*, Barcelona, Spain, 2005, pp. 3588-3594.

[3] N. Abolhassani, R. Patel, and M. Moallem, "Needle insertion into soft tissue: A survey," *Med. Eng. Phys.*, vol. 29, no. 4, pp. 413–431, 2007.

[4] H. Kataoka, T. Washio, M. Audette, and K. Mizuhara, "A model for relations between needle deflection, force, and thickness on needle penetration," *in Proc. 4th Int. Conf. Med. Image Comput. Comput.-Assist. Intervent.,* 2001, pp. 966–974.

[5] S. Bann, M. Khan, V. Datta, and A. Darzi, "Surgical skill is predicted by the ability to detect errors," *The American Journal of Surgery*, vol. 189, no. 4, pp. 412-415, 2005.

[6] Y-L. Park, et al. "MRI-compatible Haptics: Strain sensing for real-time estimation of three dimensional needle deflection in MRI environments." *Int. Society for Magnetic Resonance in Medicine, 17th Scientific Meeting and Exhibition*, Honolulu, Hawaii. 2009.

[7] K. Rebello, "Applications of MEMS in Surgery.*" Proceedings of the IEEE*, vol. 92 no. 1, pp. 43-55, 2004.

[8] Z. Sun, M. Balicki, J. Kang, J. Handa, R. Taylor, and I. Iordachita, "Development and preliminary data of novel integrated optical micro-force sensing tools for retinal microsurgery," in *Proc. 2009 IEEE Int. Conf. Robot. Autom.*, 2009, pp. 1897–1902.

[9] F. Hammond, R. Kramer, Q. Wan, R. Howe, and R. Wood, "Soft Tactile Sensors for Micromanipulation," *IEEE Int. Conf. on Intelligent Robotics and Systems*, Vilamoura, Portugal, pp. 25-32, 2012.

[10] S. Timoshenko and D. H. Young, Engineering Mechanics, 4th ed. New York: McGraw-Hill, 1956.

[11] T. Chaikeeree et. al, "An Anlaysis of RF Sputtering Power and Argon Gas Pressure Affecting on ITiO Films Characteristics," *J. of Energy Technologies and Policy*, vol. 3, no. 11, pp. 240-245, 2013.

[12] ATI Industrial Automation Inc., "Silicon or Foil: Which Strain Gage should be used in Force/Torque Sensors?" *Technical Report*, Available: http://www.dfe.com/pdfs/Silicon-vs-Foil.pdf.

[13] Y. Shixuan and N. Lu, "Gauge Factor and Stretchability of Silicon-on-Polymer Strain Gauges," *Sensors,* vol. 13, no. 7, pp. 8577-8594, 2013.